Hindawi
International Journal of RF and Microwave Computer-Aided Engineering
Volume 2023, Article ID 6682038, 10 pages
https://doi.org/10.1155/2023/6682038

Research Article

Wideband Dual-Polarized Differential-Fed Filtering Microstrip Patch Antenna with High Suppression and Wide Stopband

Quanwei Wu, Yan Shi, and Long Li

School of Electronic Engineering, Xidian University, Xi'an, 710071 Shaanxi, China

Correspondence should be addressed to Yan Shi; shiyan@mail.xidian.edu.cn

Received 20 January 2023; Revised 14 March 2023; Accepted 3 April 2023; Published 13 April 2023

Academic Editor: Piotr Gas

This paper presents a wideband dual-polarized filtering antenna with high suppression level and wide stopband. In the proposed antenna, the driven patch operates in a TM10 mode with an inherent radiation null caused by a higher mode TM12. Four dual-strip structures connected with the feeding probes are placed below the driven patch to achieve the capacitive coupling, thus resulting in a low-frequency radiation null with a sharp roll-off rate. The introduction of the parasitic patch and strips generates an in-band resonance and two high-frequency radiation nulls, which widens the upper stopband. Four slots are etched on the driven patch to excite the third resonance, thus achieving the wide operation band. The prototype of the proposed antenna is fabricated. With four controllable radiation nulls, the out-of-band suppression levels are above 29 dB in low-frequency band greater than 1 GHz and above 21 dB in high-frequency band up to 7 GHz, respectively. Due to the three in-band resonances, a wide impedance bandwidth of 2.93-3.96 GHz with a fractional band of 30% is obtained. With the rotational symmetry structure driven by differential probes, the proposed dual-polarized antenna has a cross-polarization ratio better than 28 dB, a high polarization isolation above 43 dB, and a good peak gain about 9.9 dBi.

1. Introduction

With the rapid application of massive multiple-input multiple-output (MIMO) technology in the fifth-generation (5G) wireless communication, architecture of RF front end becomes extraordinarily complicated. Thus, high demands on antenna including multiple functions, high integration, and good performance are put forward. On the one hand, channel capacity can be greatly improved by broadening operational band and utilizing polarization diversity, and therefore, wideband dual-polarized performance becomes necessary for the base station antenna arrays. On the other hand, good polarization characteristics and isolation are significant for the anti-interference ability of the system. By introducing differential circuit with common mode suppression, the circuit noise can be effectively reduced, and meanwhile, the stability of the pattern can be greatly improved. However, bulky volume of the RF front end by cascading the antenna with the filter for the interference suppression is still a problematic issue. Integration of the antenna and the filter, called filtering antenna, becomes a feasible way to reduce the volume of the RF front end.

Among the filtering antenna designs, fusion design for the filtering antennas becomes popular. Specifically, radiation nulls can be generated by reasonably introducing some specific structures into the antenna [1, 2]. Based on the fusion design, various filtering antennas have been proposed, for instance, wideband filtering antennas [3–6] and filtering antennas with good selectivity characteristic including steep roll-off [7–12], good suppression level [13–19], and wide stopband [20–23]. In [3], an E-shaped grounded feeding structure and four stepped impedance resonators are used to excite three resonance modes to obtain a wide fractional band of 22.2%. But the skirt selectivity is not good enough by integrating the resonators with the feedlines. In [8], good selectivity is achieved by a dual-probe feeding structure according to the cascaded quadruplet (CQ) cross coupling. However, the obtained suppression level is only about 15 dB. In [22], four short strips and a long cross-type strip together with a square ring slot are used to generate two

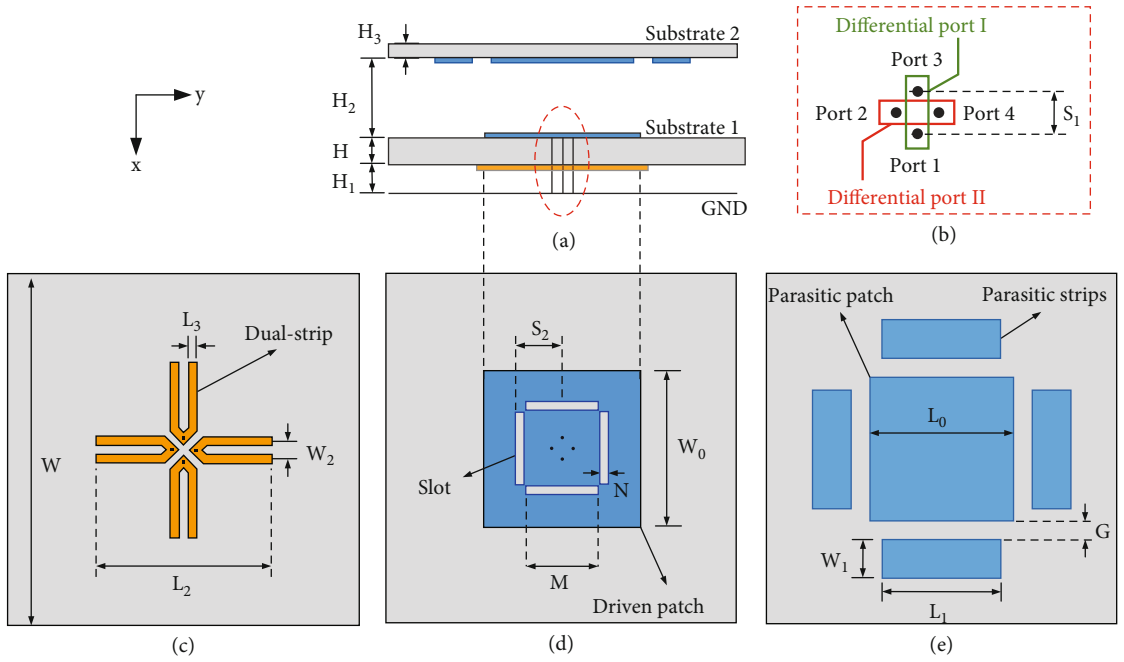

FIGURE 1: Configuration of the proposed filtering antenna. Geometric parameters of the antenna are as follows (unit: mm): $W = 80$, $W_0 = 29.1$, $W_1 = 7$, $W_2 = 3$, $L_0 = 26.7$, $L_1 = 22$, $L_2 = 30$, $L_3 = 1.5$, $G = 3.5$, $S_1 = 4$, $S_2 = 8.7$, $M = 13.5$, $N = 1.7$, $H = 2$, $H_1 = 1.5$, $H_2 = 6$, and $H_3 = 1$.

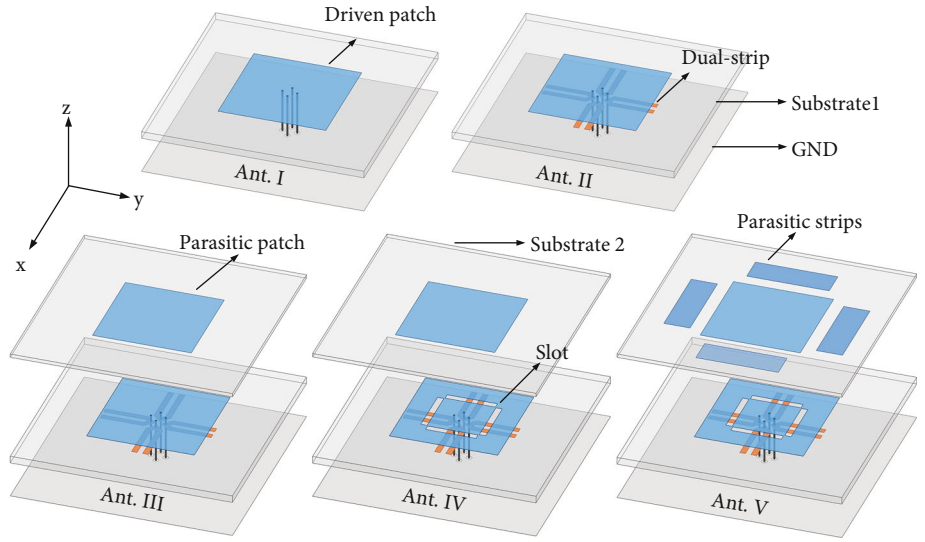

FIGURE 2: The design procedure from antenna I to antenna II to antenna III to antenna IV to proposed antenna. The geometric dimensions of each antenna are as follows (unit: mm): $W_0 = 30.7$, $H_1 = 2$, and $S_1 = 6$ for antenna I; $W_0 = 32.5$, $H_1 = 2$, $S_1 = 3.4$, and $L_2 = 32.4$ for antenna II; $W_0 = 30.7$, $H_1 = 2$, $S_1 = 2.6$, $L_3 = 1.3$, and $L_0 = 29$ for antenna III; and $W_0 = 29.7$, $H_1 = 2$, $L_2 = 30.6$, $L_3 = 1.3$, $L_0 = 28$, $S_2 = 9.9$, $M = 14$, and $N = 1.5$ for antenna IV.

radiation nulls, and thus, the upper stopband is up to 2.6 f_0 (f_0 is center frequency of the antenna). However, the simulated suppression level at the far stopband gradually becomes worse, i.e., 14 dB at 2.6 f_0. Therefore, according to the above reported fusion designs, it is still a challenging issue to design a wideband filtering antenna with good skirt selectivity and wide stopband.

In this paper, a wideband differential-fed dual-polarized filtering antenna has been designed. Four controllable radiation nulls are generated by the driven patch with the slots, the dual-strip structure, and the parasitic patch and strips, thus achieving the steep roll-off rate at the lower band edge and a wide high-frequency stopband with good suppression level, i.e., above 21 dB in high-frequency band up to 7 GHz. Moreover, three in-band resonances are excited to obtain a wide operation band of 2.93-3.96 GHz, and two pairs of the differential probes are used to achieve a low cross-polarization ratio above 28 dB and a high polarization isolation above 43 dB.

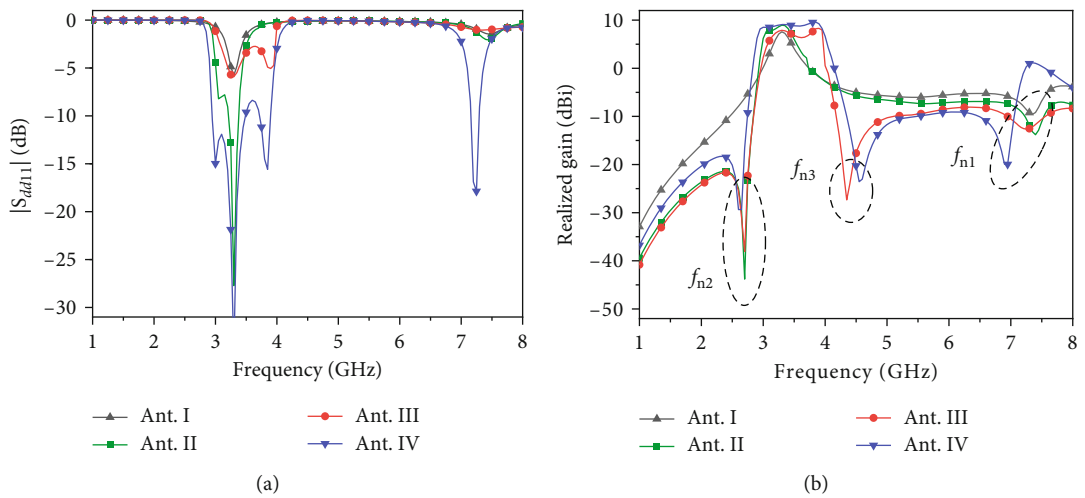

FIGURE 3: The (a) $|S_{dd11}|$ and (b) realized gain of antennas I, II, III, and IV.

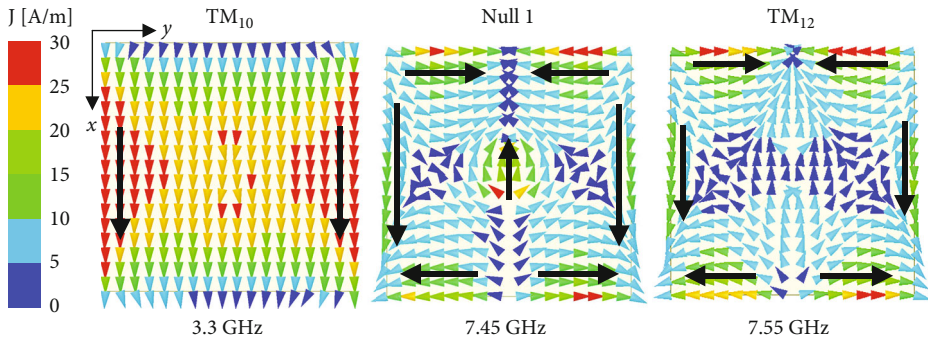

FIGURE 4: Surface current distributions on the driven patch of the antenna I.

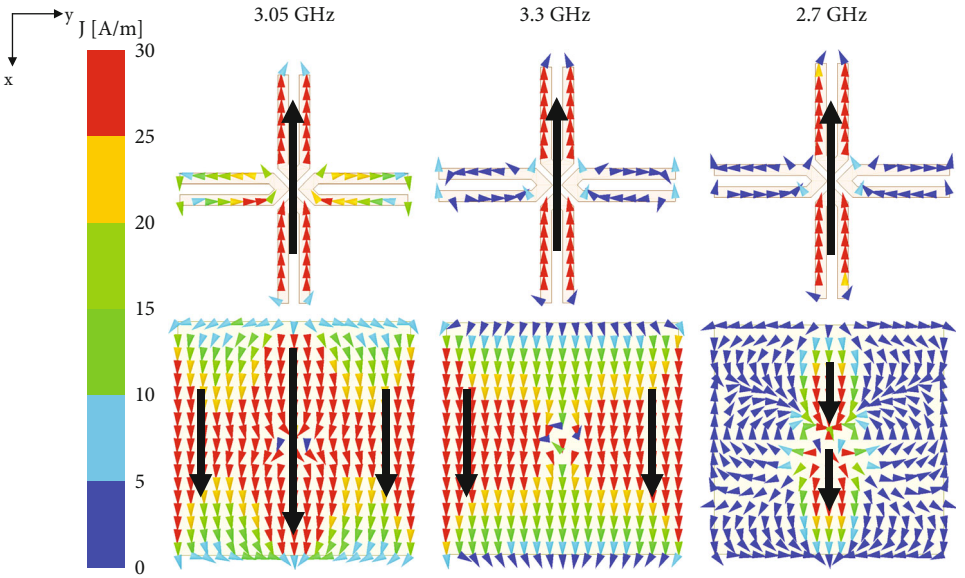

FIGURE 5: Surface current distributions on the dual strips and the driven patch of the antenna II.

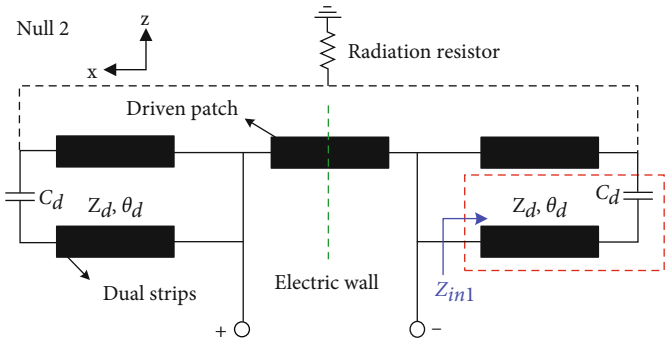

Figure 6: Equivalent circuit of the antenna II at 2.7 GHz.

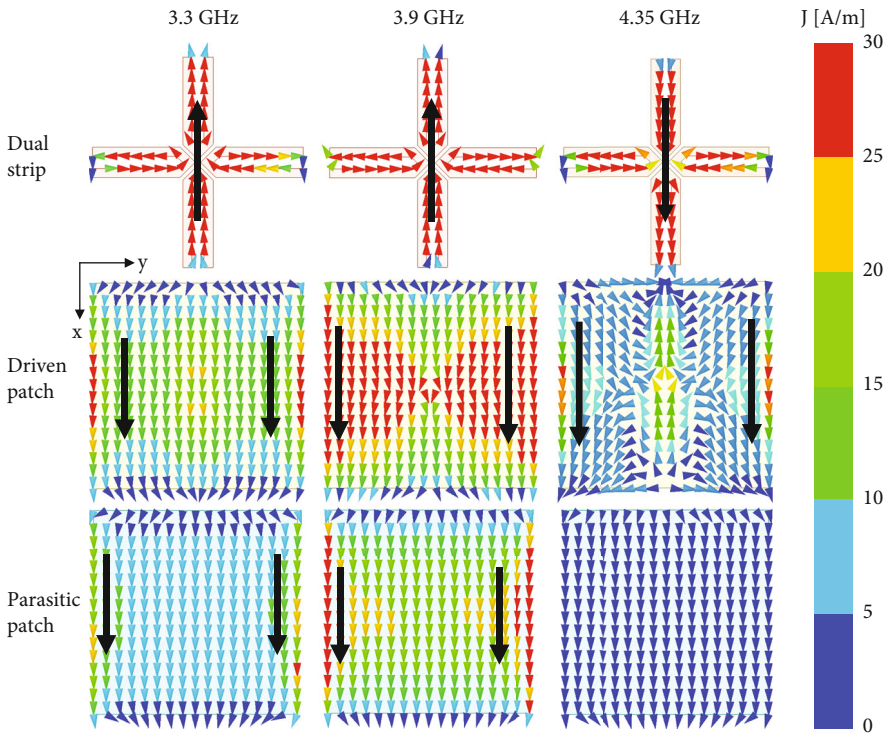

Figure 7: Surface current distributions on the dual strip, the driven patch, and the parasitic patch of the antenna III.

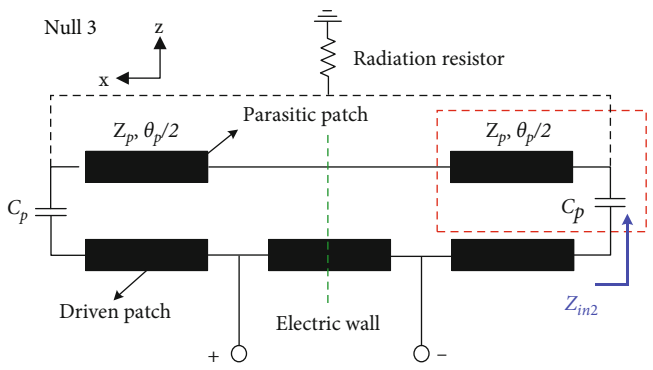

Figure 8: Equivalent circuit of the antenna III at 4.35 GHz.

2. Filtering Antenna Design

This section includes the antenna configuration, the stepping process of the proposed antenna, and the analysis of resonances and radiation nulls.

2.1. Filtering Antenna Configuration. Figure 1 shows the proposed filtering antenna, which is a stacked structure composed of the ground and the top and bottom F4B substrates with relative permittivity of 2.65 and loss tangent of 0.001. Two air layers are placed between the top and bottom substrates and the ground, respectively. A parasitic patch enclosed by four parasitic strips is fabricated on the bottom surface of the top substrate, and the driven patch and four dual strips are fabricated on the top and bottom surfaces of the bottom substrate, respectively. Four square slots are etched on the driven patch. Two pairs of differential probes,

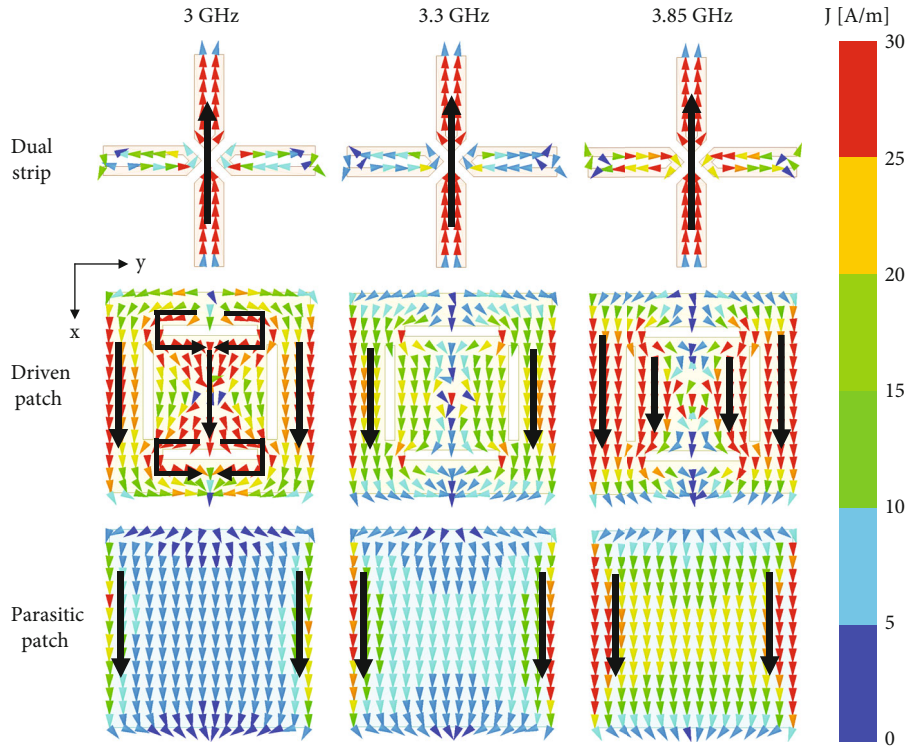

FIGURE 9: Surface current distributions on the dual strip, the driven patch, and the parasitic patch of the antenna IV.

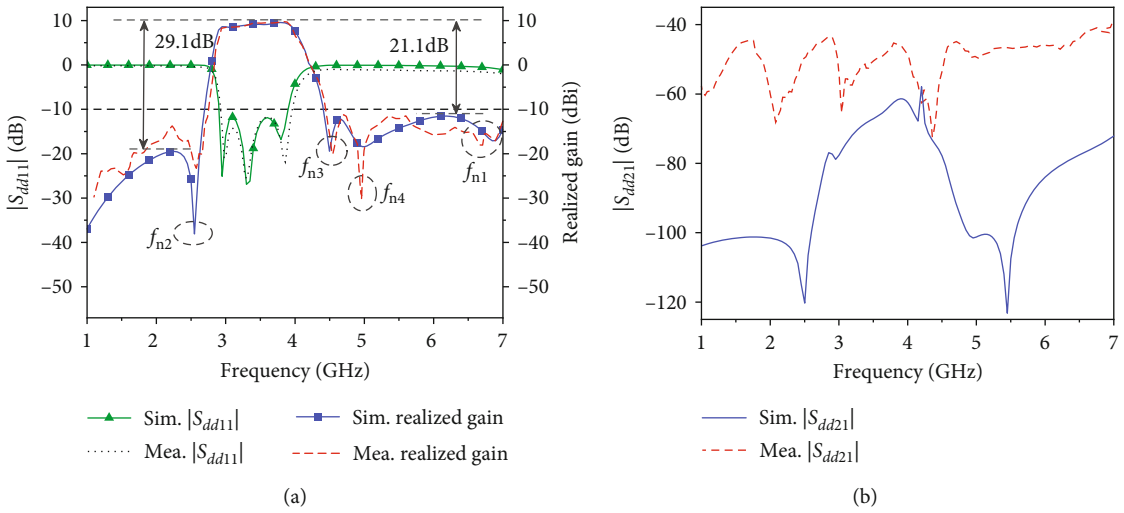

FIGURE 10: Simulated and measured (a) $|S_{dd11}|$, realized gain, and (b) $|S_{dd21}|$ of the proposed antenna.

i.e., differential port 1 consisting of ports 1 and 3 and differential port 2 consisting of ports 2 and 4, are connected with the driven patch through the four dual strips.

2.2. Operating Mechanism

2.2.1. Analysis of the Antenna I. To clearly elaborate the working mechanism and design procedure of the proposed filtering antenna, we start with the antenna I shown in Figure 2. The antenna I is a differential-fed dual-polarized patch antenna. Due to the use of the differential feeding ports I (ports 1 and 3) and II (ports 2 and 4), the resulting differential *S*-parameters are given as [2]

$$\begin{cases} S_{\mathrm{dd11}} = \dfrac{S_{11} - S_{13} - S_{31} + S_{33}}{2}, \\ S_{\mathrm{dd22}} = \dfrac{S_{22} - S_{24} - S_{42} + S_{44}}{2}, \\ S_{\mathrm{dd21}} = \dfrac{S_{21} - S_{23} - S_{41} + S_{43}}{2}, \\ S_{\mathrm{dd12}} = \dfrac{S_{12} - S_{14} - S_{32} + S_{34}}{2}. \end{cases} \quad (1)$$

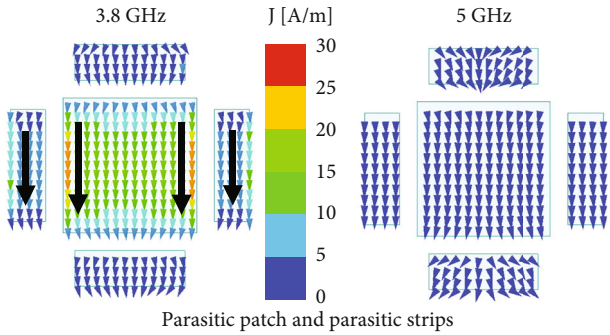

FIGURE 11: Surface current distributions on the parasitic patch and parasitic strips of the proposed antenna.

Figure 3 shows the $|S_{dd11}|$ and realized gain of the antenna I. Here, the realized gain is defined as the $(1 - |S_{dd11}|^2) \cdot G_{peak}$, with the peak gain G_{peak}. A resonance at 3.3 GHz is observed. Also, there is an inherent transmission null at 7.45 GHz. Figure 4 shows the surface currents of antenna I at 3.3 GHz and 7.45 GHz. At 3.3 GHz, the TM_{10} mode is excited. At 7.45 GHz, the surface current distribution is similar to that of the higher mode TM_{12} at 7.55 GHz shown in Figure 4. On the edge of the patch, the current along the y-direction cancels each other, whereas the current along the x-direction cancels with the current at the center of the patch. Therefore, the inherent radiation null is caused by the higher mode TM_{12}.

2.2.2. Analysis of the Antenna II. The antenna II is obtained by placing four dual strips connected with the feeding probes below the driven patch of the antenna I. An extra resonance at 3.05 GHz is excited besides the resonance at 3.3 GHz. Meanwhile, a low-frequency radiation null is generated at $f_{n2} = 2.7$ GHz. Figure 5 shows the surface current distributions of the antenna II. At 3.05 GHz, there is a strong current on the driven patch right above the dual strips because of the capacitive coupling between them. At 2.7 GHz, a weak current on the driven patch is observed. For the analysis of the generation of the radiation null, the corresponding equivalent circuit is given in Figure 6. Considering the differential feeding operation for the probe pair (1, 3) and the matching operation for the probe pair (2, 4), there is an electric wall in the middle of the antenna structure. The structure is symmetry in terms of the electric wall. Therefore, two dual strips connected to the probes 1 and 3, respectively, appears as two transmission line (TL) segments, and the driven patch is regarded as three TL segments. The TL related to the dual strip is capacitively coupled with the TL related to the driven patch by the capacitor C_d. If we ignore the effect of C_d, the structure shown in the red-dashed box of Figure 6 is reduced to a transmission line with an open terminal, with its input impedance

$$Z_{in1} = -jZ_d \cot \theta_d, \tag{2}$$

where Z_d represents the characteristic impedance of the dual strip, $\theta_d = \beta L_d$ indicates the electrical length of one strip, and L_d and β are the length and propagating constant of one strip, respectively. When θ_d is chosen as

$$\theta_d = \sqrt{\varepsilon_e}\frac{2\pi L_d}{\lambda_{null}} = \frac{\pi}{2}, \tag{3}$$

one has $Z_{in1} = 0$, meaning that the input port is shorted. Thus, the electromagnetic energy from the input port is reflected. The equivalent circuit in Figure 6 is regarded as a band-stop circuit with the resonant frequency corresponding to the radiation null

$$f_{n2} = \frac{c}{4L_d\sqrt{\varepsilon_e}}, \qquad L_d = \frac{\left[L_2 - S_1 + \left(\sqrt{2} - 1\right)W_2\right]}{2}, \tag{4}$$

where c is the speed of light in vacuum and ε_e is the effective relative permittivity.

2.2.3. Analysis of the Antenna III. Furthermore, a parasitic patch is placed above the driven patch to form the antenna III. As shown in Figure 3, there are two in-band resonances at 3.3 GHz and 3.9 GHz. Meanwhile, a new high-frequency radiation null at $f_{n3} = 4.35$ GHz is generated. When the parasitic patch is introduced, the resonance of the antenna II at 3.05 GHz moves towards the resonance at 3.3 GHz, and finally, two resonances are merged together to form the resonance of the antenna III at 3.3 GHz. In addition, a new resonance at 3.9 GHz is generated by the capacitive coupling between the driven patch and the parasitic patch. As shown in Figure 7, strong currents at 3.3 GHz and 3.9 GHz distribute on the parasitic patch, thus resulting in the good radiation. By comparison, at 4.35 GHz, very weak current on the parasitic patch is observed. The corresponding equivalent circuit is given in Figure 8, without the considerations of the dual strips. Similarly, the parasitic patch is regarded as two TL segments, and the coupling between the parasitic patch and the driven patch appears as the capacitors C_p. The structure inside the red-dashed box of Figure 8 has the following input impedance:

$$Z_{in2} = \frac{1}{j\omega C_p} + jZ_p \tan\frac{\theta_p}{2}, \tag{5}$$

where Z_p and θ_p represent the characteristic impedance and electric length of the parasitic patch, respectively. When $\omega C_p << 1$, the effect of C_p can be neglected. In this case, if θ_p is set as

$$\theta_p = \sqrt{\varepsilon_e}\frac{2\pi L_0}{\lambda_{null}} = \pi, \tag{6}$$

one has $Z_{in2} = 0$. Therefore, no energy is coupled from the driven patch to the parasitic patch. The circuit shown in Figure 8 is equivalent to a band-stop circuit, and its resonant frequency corresponding to the radiation null is

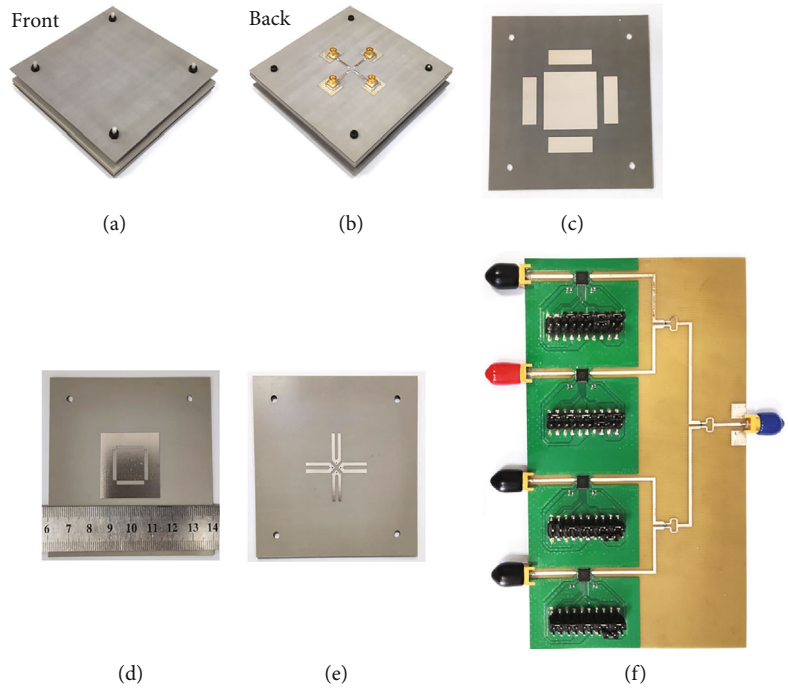

FIGURE 12: Photographs of the proposed filtering antenna: (a) 3D view (front), (b) 3D view (back), and (c) bottom view of the top substrate, (d) top view and (e) bottom view of the bottom substrate, and (f) digital phase shifter.

given as

$$f_{n3} = \frac{c}{2L_0\sqrt{\varepsilon_e}}. \tag{7}$$

2.2.4. Analysis of the Antenna IV. The antenna IV is generated by etching four slots on the driven patch. As shown in Figure 3, there are three in-band resonances at 3 GHz, 3.3 GHz, and 3.85 GHz. Moreover, the inherent radiation null shifts from 7.3 GHz to 6.9 GHz, and the radiation null at f_{n3} slightly moves towards higher frequency, which improves the high-frequency suppression. The radiation null at f_{n2} is kept unchanged. With the slots, there is a capacitive coupling between the dual strips and the parasitic patch, thus resulting in the resonance at 3 GHz, which is similar to that of the antenna II at 3.05 GHz. Figure 9 shows that at each resonance frequency, the strong current flows on the dual strips, the driven patch, and the parasitic patch.

2.2.5. Analysis of the Antenna V. Finally, the four parasitic strips are placed around the parasitic patch to form the proposed antenna, i.e., antenna V. Figure 10 shows the simulated $|S_{\mathrm{dd11}}|$, $|S_{\mathrm{dd21}}|$, and realized gain of the proposed antenna. Three in-band resonances and three out-of-band radiation nulls are kept unchanged. With the parasitic strips, a new radiation null at $f_{n4} = 5$ GHz is generated. Note that the size of the ground is the same as that of the top substrate. When only appropriately decreasing the size of the ground, the performance of the proposed filtering antenna approximately is kept unchanged. The surface current distribution is shown in Figure 11. A weak current on the parasitic strips is observed at f_{n4}. By comparison, the stronger current flows on the parasitic strips, thus resulting in the radiation at 3.8 GHz. The equivalent circuit of the radiation null at 5 GHz is the same as that of the radiation null 3. In this scenario, the capacitor C_p represents the coupling between the driven patch and the parasitic strips. Similarly, when neglecting the C_p, the electric length of the half parasitic strip $\theta_p/2$ is approximately chosen as one-quarter wavelength at f_{n4} and the input impedance of the transmission line corresponding to the parasitic strip is infinite. Therefore, the electromagnetic energy cannot be radiated by the parasitic strips.

3. Fabrication and Measurement

The prototype of the designed filtering antenna is fabricated, as shown in Figure 12. And Figure 10 shows the measured $|S_{\mathrm{dd11}}|$, realized gain, and $|S_{\mathrm{dd21}}|$. Note that the S-parameters are measured and the differential S-parameters $|S_{\mathrm{dd11}}|$ and $|S_{\mathrm{dd21}}|$ are calculated by the measured S-parameters according to Equation (1). The reflection coefficient S_{ii} ($i = 1 \sim 4$) is measured with all ports terminated with 50 Ω loads except the ith port, and the transmission coefficient S_{ij} ($i, j = 1 \sim 4$ and $i \neq j$) is measured with all ports terminated with 50 Ω loads except the ith and jth ports. The measured impedance bandwidth for $|S_{\mathrm{dd11}}| \leq -10$ dB covers 2.93~3.96 GHz (30%), in good agreement with the simulated one of 2.9~3.9 GHz (29.4%). The measured realized gain of 9.9 dBi agrees well with the simulated one of 9.6 dBi. When measuring the x-polarized realized gain, the ports 1 and 3 are excited by two signals with the equal magnitude and 180° out of phase, which is achieved by the digital phase shifter shown in Figure 12(f), with the ports 2 and 4

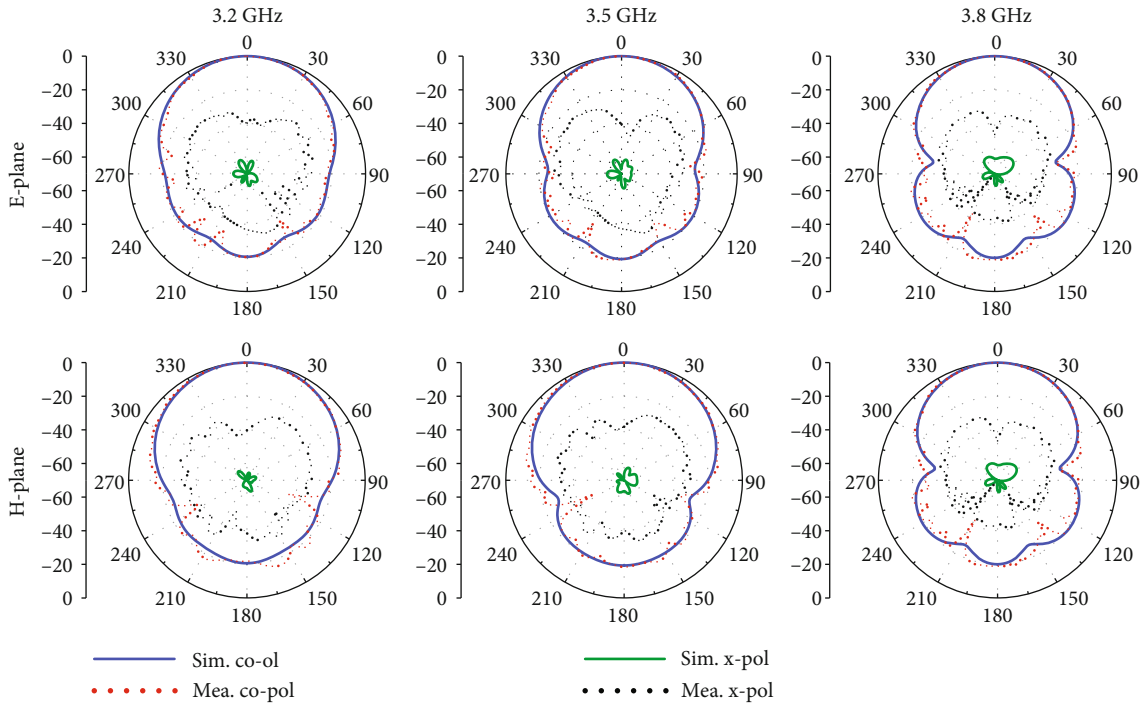

FIGURE 13: Simulated and measured normalized radiation patterns of the proposed antenna in *E*-plane and *H*-plane at 3.2 GHz, 3.5 GHz, and 3.8 GHz.

TABLE 1: Measured performance comparison with reported dual-polarized filtering antenna.

Ref.	Center frequency (GHz)	Fractional bandwidth	Gain (dBi)	Pol-isolation (dB)	Suppression level (dB)	-10 dB upper stopband	Size (λ_0^3)
[3]	3.51	22% (VSWR ≤ 1.5)	8.4 (peak)	>35.2	18.5	1.7 f_0	0.76 × 0.76 × 0.15
[4]	3.83	27.6% ($\|S_{11}\|$ ≤ −15 dB)	8.2 (average)	>25	20	1.44 f_0	0.77 × 0.77 × 0.12
[13]	2.62	12% ($\|S_{11}\|$ ≤ −15 dB)	9 (average)	>29	24	1.7 f_0	1.05 × 1.05 × 0.1
[15]	3.75	24%	8 (peak)	>20	16	2.3 f_0	0.54 × 0.73 × 0.14
[22]	2.55	15%	8.4 (peak)	>30	15.4	1.2 f_0	0.64 × 0.64 × 0.08
[23]	2.6	23%	8.9 (peak)	>26	20	1.9 f_0	0.87 × 0.87 × 0.07
This	3.45	30%	9.9 (peak)	>43	21	2.1 f_0	0.92 × 0.92 × 0.12

connected with 50 Ω loads. Similarly, for the *y*-polarized realized gain, the differential port II including the ports 2 and 4 is excited by two signals with the equal magnitude and 180° out of phase with the differential port I including the ports 1 and 3 terminated with 50 Ω loads. The measured suppression levels are better than 24 dB at the low-frequency band greater than 1 GHz and 21 dB at the high-frequency band up to 7 GHz, respectively, whereas the simulated results are 29.1 dB and 21.1 dB, respectively, in the same band. The measured polarization isolation $|S_{dd21}|$ in the band of 1~7 GHz is better than 40 dB, which is worse than the simulated one better than 58 dB. The discrepancy between the simulation and the measurement is due to the errors in the fabrication and soldering processes. In spite of the discrepancy, the measured $|S_{dd21}|$ is still very small, meaning there is a good polarization isolation of the proposed design.

Figure 13 gives the simulated and measured normalized radiation patterns in the *E*-plane and *H*-planes at 3.2 GHz, 3.5 GHz, and 3.8 GHz. The simulated and measured copolarized components agree well with each other. The measured and simulated cross-polarized ratios are 28 dB and 56 dB, respectively. The discrepancy between the measurement and the simulation is due to the fabrication and measurement errors including soldering and assembling technology, substrate material tolerance, and antenna installation.

Table 1 gives the measured performance comparison between the previously reported dual-polarized filtering antenna and the proposed design. The proposed antenna has a wider operation band (30%), a higher gain (9.9 dBi),

a lower polarization isolation (43 dB), and a wider upper stopband (2.1 f_0). Here, f_0 is the center frequency of the operating band. It is worthwhile pointing out that the proposed filtering antenna can be arranged into an array for the application of the multiantenna communication. In this scenario, besides the reasonable consideration of the array layout, the decoupling structures should be used to reduce the mutual decoupling between the antenna elements, which will be our next research work.

4. Conclusion

In this paper, a dual-polarized differential-fed filtering antenna has been developed. The dual strips connected to the fed probes are used to realize a band-stop response, thus leading to a low-frequency radiation null with a high suppression level. The parasitic structures including the patches and the strips generate two high-frequency radiation nulls and cooperate with the inherent radiation null caused by the higher-order modes of the driven patch to greatly widen the upper stopband. Meanwhile, the interaction between the driven patch with the slots and the parasitic patches results in three in-band resonances to achieve a wide operation band. The proposed filtering antenna well operates in n78 band and effectively suppresses the interferences from GSM, CDMA, LTE, and Bluetooth communication bands. In addition, the high polarization isolation between the dual polarization differential ports and good cross-polarization ratio is also achieved. With these good performance, the proposed filtering antenna has a wide application prospect in 5G communication system.

Data Availability

The data used to support the findings of this study are included within the article.

Conflicts of Interest

The authors declare that they have no conflicts of interest.

Acknowledgments

This work was supported by the National Key Research and Development Program of China (no. 2021YFA1401001).

References

[1] W. C. Yang, S. Chen, Q. Xue, W. Q. Che, G. X. Shen, and W. J. Feng, "Novel filtering method based on metasurface antenna and its application for wideband high-gain filtering antenna with low profile," *IEEE Transactions on Antennas and Propagation*, vol. 67, no. 3, pp. 1535–1544, 2019.

[2] X. J. Yang, L. Ge, J. P. Wang, and C. Sim, "A differentially driven dual-polarized high-gain stacked patch antenna," *IEEE Antennas and Wireless Propagation Letters*, vol. 17, no. 7, pp. 1181–1185, 2018.

[3] Y. P. Li, Z. P. Zhao, Z. Y. Tang, and Y. Z. Yin, "Differentially-fed, wideband dual-polarized filtering antenna with novel feeding structure for 5G sub-6 GHz base station applications," *IEEE Access.*, vol. 7, pp. 184718–184725, 2019.

[4] S. J. Yang, Y. M. Pan, Y. Zhang, Y. Gao, and X. Y. Zhang, "Low-profile dual-polarized filtering magneto-electric dipole antenna for 5G applications," *IEEE Transactions on Antennas and Propagation*, vol. 67, no. 10, pp. 6235–6243, 2019.

[5] P. F. Hu, Y. M. Pan, X. Y. Zhang, and S. Y. Zheng, "Broadband filtering dielectric resonator antenna with wide stopband," *IEEE Transactions on Antennas and Propagation*, vol. 65, no. 4, pp. 2079–2084, 2017.

[6] Y. Zhang, X. Y. Zhang, and Q. H. Liu, "Dual-polarized filtering magnetoelectric dipole antenna utilizing intrinsic highpass filter network and integrated lowpass filter network," *IEEE Transactions on Antennas and Propagation*, vol. 69, no. 12, pp. 8090–8099, 2021.

[7] Y. P. Li, Z. P. Zhao, Z. Y. Tang, and Y. Z. Yin, "Differentially fed, dual-band dual-polarized filtering antenna with high selectivity for 5G sub-6 GHz base station applications," *IEEE Transactions on Antennas and Propagation*, vol. 68, no. 4, pp. 3231–3236, 2020.

[8] K. R. Xiang, F. C. Chen, Q. Tan, and Q. X. Chu, "High-selectivity filtering patch antennas based on multipath coupling structures," *IEEE Transactions on Microwave Theory and Techniques*, vol. 69, no. 4, pp. 2201–2210, 2021.

[9] C. Y. Wang, X. Wang, H. W. Liu, Z. J. Chen, and Z. W. Han, "Substrate integrated waveguide filtenna with two controllable radiation nulls," *IEEE Access.*, vol. 8, pp. 120019–120024, 2020.

[10] Y. M. Pan, P. F. Hu, X. Y. Zhang, and S. Y. Zheng, "A low-profile high-gain and wideband filtering antenna with metasurface," *IEEE Transactions on Antennas and Propagation*, vol. 64, no. 5, pp. 2010–2016, 2016.

[11] D. Yang, H. Q. Zhai, C. Z. Guo, and H. K. Li, "A compact single-layer wideband microstrip antenna with filtering performance," *IEEE Antennas and Wireless Propagation Letters*, vol. 19, no. 5, pp. 801–805, 2020.

[12] S. J. Yang, Y. M. Pan, L. Y. Shi, and X. Y. Zhang, "Millimeter-wave dual-polarized filtering antenna for 5G application," *IEEE Transactions on Antennas and Propagation*, vol. 68, no. 7, pp. 5114–5121, 2020.

[13] W. Duan, X. Y. Zhang, Y. M. Pan, J. X. Xu, and Q. Xue, "Dual-polarized filtering antenna with high selectivity and low cross polarization," *IEEE Transactions on Antennas and Propagation*, vol. 64, no. 10, pp. 4188–4196, 2016.

[14] W. Wang, Z. Zheng, X. C. Fan et al., "A waveguide slot filtering antenna with an embedded metamaterial structure," *IEEE Transactions on Antennas and Propagation*, vol. 67, no. 5, pp. 2953–2960, 2019.

[15] K. Xue, D. Yang, C. Z. Guo, H. Q. Zhai, H. K. Li, and Y. Zeng, "A dual-polarized filtering base-station antenna with compact size for 5G applications," *IEEE Antennas and Wireless Propagation Letters*, vol. 19, no. 8, pp. 1316–1320, 2020.

[16] J. Y. Jin, S. W. Liao, and Q. Xue, "Design of filtering-radiating patch antennas with tunable radiation nulls for high selectivity," *IEEE Transactions on Antennas and Propagation*, vol. 66, no. 4, pp. 2125–2130, 2018.

[17] C. K. Lin and S. J. Chung, "A filtering microstrip antenna array," *IEEE Transactions on Microwave Theory and Techniques*, vol. 59, no. 11, pp. 2856–2863, 2011.

[18] N. Nie and Z. H. Tu, "Wideband filtering dumbbell-shaped slot antenna with improved frequency selectivity for both band-edges," *IEEE Access.*, vol. 8, pp. 121479–121485, 2020.

[19] B. H. Zhang and Q. Xue, "Filtering antenna with high selectivity using multiple coupling paths from source/load to resonators," *IEEE Transactions on Antennas and Propagation*, vol. 66, no. 8, pp. 4320–4325, 2018.

[20] F. C. Chen, R. S. Li, and Q. X. Chu, "Ultra-wide stopband low-pass filter using multiple transmission zeros," *IEEE Access.*, vol. 5, pp. 6437–6443, 2017.

[21] J. F. Qian, F. C. Chen, Y. H. Ding, H. T. Hu, and Q. X. Chu, "A wide stopband filtering patch antenna and its application in MIMO system," *IEEE Transactions on Antennas and Propagation*, vol. 67, no. 1, pp. 654–658, 2019.

[22] M. Z. Xun, W. C. Yang, W. J. Feng, Y. Q. Zhang, Q. Xue, and W. Q. Che, "A differentially fed dual-polarized filtering patch antenna with good stopband suppression," *IEEE Transactions on Circuits and Systems II: Express Briefs*, vol. 68, no. 4, pp. 1228–1232, 2021.

[23] W. C. Yang, M. Z. Xun, W. Q. Che, W. J. Feng, Y. Q. Zhang, and Q. Xue, "Novel compact high-gain differential-fed dual-polarized filtering patch antenna," *IEEE Transactions on Antennas and Propagation*, vol. 67, no. 12, pp. 7261–7271, 2019.